Applied Materials Today 19 (2020) 100543

Contents lists available at ScienceDirect

Applied Materials Today

journal homepage: www.elsevier.com/locate/apmt

Selective laser melting manufactured porous Fe-based metallic glass matrix composite with remarkable catalytic activity and reusability

Shun-Xing Liang [a], Xueqing Wang [a], Wenchang Zhang [b], Yu-Jing Liu [a,*], Weimin Wang [c,**], Lai-Chang Zhang [a,*]

[a] School of Engineering, Edith Cowan University, 270 Joondalup Drive, Joondalup, Perth, WA 6027, Australia
[b] Ji'an Ecological Environment Monitoring Center of Jiangxi Province, Ji'an, Jiangxi Province 343000, China
[c] School of Materials Science and Engineering, Shandong University, Jinan, Shandong Province 250061, China

ARTICLE INFO

Article history:
Received 25 June 2019
Accepted 20 December 2019

Keywords:
Selective laser melting
Metallic glass matrix composite
Catalyst
Porous microstructure
Reusability

ABSTRACT

The ever-increasing environmental consciousness has stimulated new design of catalysts to meet environmental requirements due to rapid expansion of industrialization. Additive manufacturing now emerges as a novel technology that revolutionizes the way of material manufacturing with functional applications. Herein, the manufacturing of an Fe-based metallic glass (MG) matrix composite with three-dimensional rhombic dodecahedron microstructure by selective laser melting (SLM) is reported. The SLM-produced porous Fe-based MG matrix composite has been employed into catalytic activation in Fenton-like process and sulfate radical-based reaction. Results demonstrate that up to 45 times reusability is achieved in sulfate radical-based reaction without any apparent efficiency decay, which is the highest reusability with high efficiency by catalysts as of now. The remarkable catalytic reusability originates from extremely low surface decay in sulfate radical-based reaction. In addition, structural analysis indicates the α-Fe nanocrystals could trigger easy electron transfer but a large amount of α-Fe lead to an inhibitive catalytic effect in the MG matrix composite. The overall catalytic ability also demonstrates the excellent catalytic performance of SLM-produced porous Fe-based MG matrix composite in the wastewater remediation. This work suggests a novel SLM-produced catalyst with promising industrial potential and value.

1. Introduction

In recent years, the growing severe environmental problems after entering 21 st century have stimulated the new design of catalysts with advantages of low cost, customization and accommodation of practical applications. Additive manufacturing (AM), also known as three-dimensional (3D) printing, has become a new technology to simplify material manufacturing in a single process [1,2]. Compared with traditional manufacturing process, AM technology is mostly based on the bottom-up (incremental addition of layers of materials) process [3,4], which contributes to the time-saving and cost-effective preparation of complex 3D structure. At the same time, by engineering their complex geometries (architecture, size, pore, surface, etc.), AM technology endows the produced component with optimized structural properties and functionality. Noting that a unique microstructure is closely related to the catalytic performance of a catalyst, AM technology thereby holds the promise to design the new generation of catalysts to meet the environmental concerns.

Current AM technologies have been reported to successfully manufacture multifunctional catalysts, such as graphene composite [5], Cu/Al_2O_3 [6] by fused deposition modelling, mixed-metal oxides [7] by inkjet printing, zeolite [8] by robocasting (or direct ink writing), and polymer composite with Ag nanoparticles [9], Mn- and Na_2WO_4-contained polymer [10] by stereolithography (or digital light processing). In addition, recent studies indicate that powder-bed-based processes including selective laser melting (SLM) and electron beam melting (EBM) have been applied to fabricate metal-based novel catalysts. For example, TiO_2 electrodes with a tunable microstructure of conical arrays were manufactured by SLM for efficient water splitting [11]; steel-IrO_2 electrodes with excellent pseudocapacitive and catalytic properties were fabricated by SLM for oxygen evolution reaction in the alkaline solutions [12]; static mixers coated with Ni or Pt were prepared by EBM

* Corresponding authors.
** Corresponding author.
E-mail addresses: liuyujing555@163.com (Y.-J. Liu), weiminw@sdu.edu.cn (W. Wang), lczhangimr@gmail.com (L.-C. Zhang).

https://doi.org/10.1016/j.apmt.2019.100543
2352-9407/

for hydrogenations of alkenes and carbonyls [13]. Given that current AM technology usually focuses on extrusion-based printing strategy to manufacture catalysts (polymers, carbon materials, zeolites, etc.), powder-bed-based processes, which are unbuildable for many materials due to high working temperature, for metal-based catalyst production are lack of sufficient demonstration and understanding. In addition, the application of AM-produced catalysts in wastewater remediation aiming to relieve environmental pressure is still embryonic.

Recently, metallic glasses (MGs or amorphous alloys) with advanced catalytic nature have attracted increasing research interests in catalytic fields owing to its disordered atomic packing structure compared to well-arranged structure in crystalline alloys [14–17]. The unique structure has stimulated MGs to be catalytically applied in water splitting, organic pollutant remediation, methanol and ethanol oxidation, hydrogenation, etc. It is now known that the fascinating catalytic abilities in MG originate from its low thermal activation energy barrier [18], fast electron transfer [19], unsaturated coordination of atomic numbers and high surface active sites [20], and self-stabilizing [21]. The superior reusability in MGs is also attracting increasing attentions, especially in the wastewater remediation, such as 30 times by $Fe_{78}Si_9B_{13}$ MG [22], 23 times by $Fe_{80}P_{13}C_7$ MG [23], 20 times by $Fe_{81}Si_2B_{10}P_6Cu_1$ MG [24] and 35 times by recent reported $Fe_{83}Si_2B_{11}P_3C_1$ MG [25]. As such, it is worth to consider amorphous structure in the design of novel catalysts. Notably, synthesis of amorphous-crystalline dual-phase microstructure has been suggested as an effective way to promote electron transfer efficiency. It was reported that the embedded nanocrystals could serve as "triggers" to induce surrounded amorphous phase, promoting the interfacial electron transfer from crystalline phase to amorphous phase [26]. This fact could be applied in Fe-based MGs, which generally have α-Fe nanocrystals after crystallization. The α-Fe nanocrystals have been reported to demonstrate a higher electrochemical activity than the amorphous counterpart [27], and thus Fe-based amorphous-crystalline composites are expected to exhibit a promising performance in the catalytic activity.

In this work, SLM was employed to manufacture a porous Fe-based MG matrix composite with complex rhombic dodecahedron microstructure by a pre-designed 3D computer-aided design (CAD) model. The Fe-based powder was selected due to the environmental-friendly, cost-effective and high catalytic nature. Although recently SLM-produced Zr-based bulk MG has been applied into wastewater treatment [28], Fe-based catalysts tend to be more active and much superior in the advanced oxidation processes (AOPs) [29,30]. The as-produced porous Fe-based MG matrix composite can be directly applied into catalytic reaction without subsequent surface and structural treatment. The demonstrated catalytic activity and reusability in SLM-produced porous Fe-based MG matrix composite as well as the combination of 3D printing and attractive amorphous-crystalline microstructure provide a new clue and a great economic value for wastewater remediation.

2. Experimental

2.1. Powder

The MG matrix composite powder with a nominal composition of $Fe_{70}Cr_5Ni_3Mo_3W_9Si_5B_5$ was manufactured by gas atomization and supplied by Beijing Sangyao Technology Development Co., Ltd. Size distribution of powder was analyzed by a particle size analyzer (Mastersizer MicroPlus, Malvern). The average particle size (d_{50}) of composite powder was 49 μm with a nominal particle size distribution between 10 and 140 μm (Fig. 1a). A small quantity of them were ranged from 220 to 260 μm in size. The Brunauer-Emmett-Teller (BET) method (by Tristar II 3020, Micromeritics) was employed to evaluate the specific surface area of composite powder, which was 0.2876 m^2/g. X-ray diffraction (XRD) pattern shows a broad diffraction peak with a range of 45 to 60°, indicating the main amorphous phase embedded with α-Fe nanocrystals in the composite powder (Fig. 1b). Differential scanning calorimetry (DSC) measurement of the composite powder demonstrates the onset crystallization temperature (T_x) as 540 ° with an exothermic enthalpy (ΔH_x) of 19.7 J/g (Fig. 1b inset), which is lower than those for other Fe-based MGs (e.g. 42.8 J/g in $Fe_{78}Si_{13}B_9$ [31] and 83.9 J/g in $Fe_{50}Ni_{30}P_{13}C_7$ [32]).

2.2. Preparation of Fe-based MG matrix composite by SLM

The SLM-produced Fe-based MG matrix composite was manufactured by a MTT SLM 250 H L machine equipped with a 400 W Yb:YAG fiber laser (wavelength of 1.06 μm and spot size of 80 μm). Prior to building the composite, Magics software (Materialize, Belgium) was used to create a 3D CAD model by repeating a single unit cell (3.33 mm × 3.33 mm × 3.33 mm in size) to produce a rhombic dodecahedron microstructure (3 × 3 × 3 array of unit cells) with a nominal porosity of 75 % (Fig. 2a). The laser power, the powder layer thickness and scan spacing were set to be 200 W, 100 μm and 100 μm, respectively. The chamber was filled with Argon gas before SLM process to avoid any contamination from oxygen. Fig. 2b shows the schematic illustration of the SLM process. Loose powder of thin layer (commonly 20–100 μm) was deposited on the substrate, followed with laser scanning melting based on pre-designed CAD model with controlled parameters in SLM machine [33]. Repeating process with layer by layer contributes to the building of whole component. It should be noted that the substrate was heated to be 200 ° to lower stress gradient between SLM-produced layer and the substrate. Since the scan speed usually plays an important role during SLM process [34,35], which affects the quality of component and may have an impact on the catalytic performance of SLM-produced component, different scan speeds (from 500 to 2000 mm/s) were selected to produce the Fe-based MG matrix composite by SLM in this work. As shown in Fig. 2c, the entire scaffolds after SLM process based on scan speeds from 500 to 2000 mm/s was depicted. The zoom-in view of component manufactured at the laser scan speed of 1250 mm/s clearly shows the good forming of final scaffold as pre-designed CAD model in Fig. 2a.

2.3. Catalytic analysis towards reusability

The catalytic performance of SLM-produced Fe-based MG matrix composite was conducted with the involvement of cibacron brilliant red 3B-A (BR3B-A) dye as organic pollutant, and hydrogen peroxide (H_2O_2, 30 % w/w) and sodium persulfate ($Na_2S_2O_8$, PS, ≥99.0 %) as peroxides, which were purchased from Sigma-Aldrich. The hydrochloric acid (HCl, 37 % w/w) and sulfuric acid (H_2SO_4, 0.5 M) were used to control pH as 3.0 throughout all the catalytic experiments. At predetermined time intervals, about 4 mL of aqueous sample was collected from the reaction solution for immediate detection by UV–vis spectrometer (Perkin Elmer Lambda 35) at absorbance peak (λ_{max}) of 517 nm. During recycling experiments, 1.9 g (weight of sample) catalyst, 1 mM peroxide (H_2O_2 or PS) and 20 ppm BR3B-A dye were used with continuous stirring under room temperature. A thermostatic water bath was used to control the constant reaction temperature. After each experiment, the MG matrix composite was collected with 2 min ultrasonic cleaning in the Milli-Q water (18.2 MΩ cm). Then it was applied into the newly prepared dye solution immediately with stirring under the same conditions. After reused for 45 times, the MG matrix composite was cleaned by absolute ethanol for further characterization. In order to analyze the effect of structural change on the correspond-

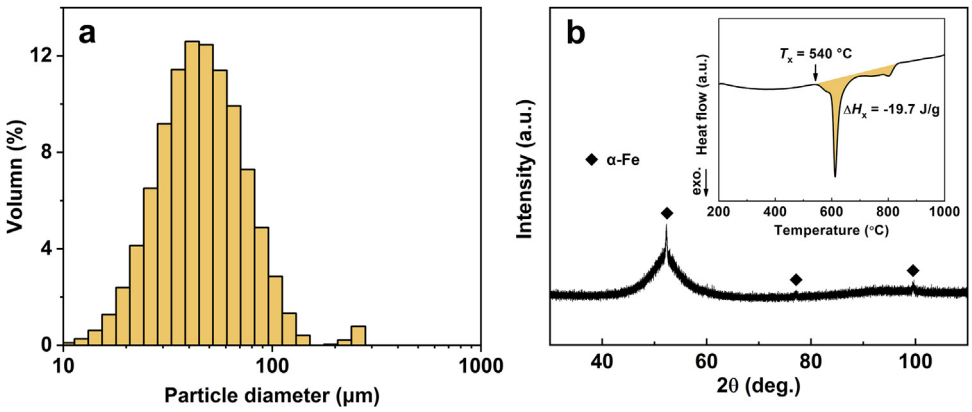

Fig. 1. (a) The particle size distribution and (b) XRD pattern of the as-produced MG matrix composite powder. Inset of (b) shows the corresponding DSC curve.

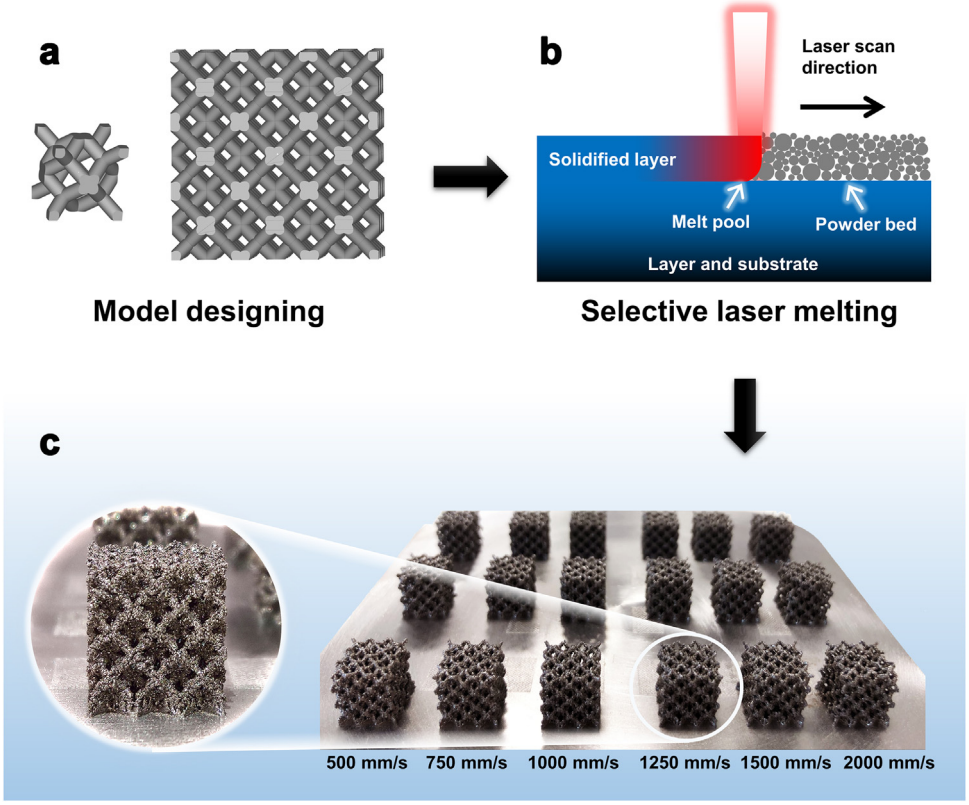

Fig. 2. (a) 3D CAD model of single unit cell and the whole rhombic dodecahedron microstructure. (b) Schematic illustration of SLM process. (c) The entire scaffolds on top of the base plate arranged by laser scan speeds from 500 to 2000 mm/s.

ing catalytic performance, the MG matrix composite was subjected to fast annealing at 550° for 5 min under the protection of Argon gas, followed with fast quenching by air cooling.

2.4. Material characterization

The microstructural features of Fe-based MG matrix composite powder and corresponding SLM-produced components were characterized by XRD using a PANalytical Empyrean diffractometer with Co-Kα radiation. The surface morphologies were observed and analyzed by scanning electron microscope (SEM) (SUPRA 55-VP, Zeiss). The thermal behavior of composite powder (i.e. T_x and ΔH_x) was investigated by DSC (DSC-404C, Netzsch) at a heating rate of 20 K/min. The thermal treatment of MG matrix composite was conducted under a tube furnace (OTF-1200X, MTI) with protection by Argon gas.

3. Results and discussion

3.1. Reusability

Reusability in MG ribbons recently has attracted extensive research interests due to their practical application value in the industry [22,23,25]. Unlike powder used as catalyst in the wastewater treatment, ribbons are more achievable in the easy operation, reduction of cost and control of excess reaction. In addition, the amorphous nature of MG ribbons has provided a strong stability regarding surface and internal microstructure, where all the pre-

vious studies about reusability of MG ribbons have demonstrated the unchangeable microstructure (without any crystallization) after being reused [22–25,36–39]. The well-maintained amorphous nature facilitates an easy electron transfer with active surface during the redox reaction. Generally, Fe-based MG ribbons can be reused for 10–20 times in the Fenton-like reaction before significant decay of catalytic efficiency, which may be attributed to severe surface deposits, surface oxidation and intrinsic mass loss after reaction. For example, the degradation efficiency of 20th time reused $Fe_{80}P_{13}C_7$ MG ribbons is about half of the 1 st use [23]; the catalytic efficiency of 16th time reused $Fe_{81}Si_2B_{10}P_6Cu_1$ MG ribbons is about one third of the 1 st use [24]. Both of them used low concentration of H_2O_2 (1 mM) as peroxide. However, the reusability of Fe-based MGs seems to be more reliable and can be extended in the sulfate radical-based reaction. For example, $Fe_{83}Si_2B_{11}P_3C_1$ MG ribbons have been reported to be reused up to 33 times before apparent decrease of efficiency in the activation of PS to degrade rhodamine B [25], which is the highest reusability as of now. Despite their diversity in chemical compositions, this provides a new clue that the reusability of MGs should present distinct behavior in Fenton-like and sulfate radical-based systems, and thus it is significant to investigate the discrepancy to extend the reusability in the current SLM-produced Fe-based MG matrix composite.

Prior to investigating the reusability of SLM-produced Fe-based MG matrix composite, the effect of different laser scan speeds on the catalytic performance were analyzed in the Fenton-like process. The catalytic efficiency was investigated by first-order kinetic model: $C/C_0 = \exp(-k_{obs}t)$ [40], where C and C_0 represent dye concentration at instant reaction time t and at the initial time t_0, respectively; k_{obs} (min^{-1}) is the reaction rate constant. According to Fig. 3a, it is apparent that the laser scan speed has an effect on the degradation efficiency of BR3B-A dye. The increase of laser scan speed generally results in the improvement of efficiency. The sample of 2000 mm/s has a decolorization rate about 20 % higher than the counterpart of 500 mm/s at 2 min, but all of them can achieve almost 100 % removal rate of dye at 10 min, indicating that the MG matrix composite has a strong ability to activate H_2O_2 to degrade dye molecules in solution. The SLM-produced Fe-based MG matrix composite has a comparable or even higher degradation efficiency than SLM-produced Zr-based ($Zr_{55}Cu_{30}Ni_5Al_{10}$) bulk MG [28,41], without chemical dealloying and high-temperature thermal activation in this work. According to the degradation performance in Fig. 3a, the SLM-produced Fe-based MG matrix composites with 2000 mm/s was selected to further investigate their reusability in different AOPs.

Fig. 3b firstly shows the SLM-produced Fe-based MG matrix composite in the Fenton-like process to degrade BR3B-A dye. After the 1 st use, the degradation efficiencies at the 2nd and 3rd use are apparently decreased but all these reactions can achieve almost complete degradation in 10 min. The decay of catalytic efficiency is easy to understand since the fresh surface of catalyst tends to be oxidized during reactions and be covered with reaction products [42]. This behavior has a similar tendency as reported from previous recycling experiments of MG ribbons [23,24]. However, although reusing MG matrix composite from 4th to 23rd times leads to further progressive decrease in degradation efficiency, the attenuation is obviously slower than the initial three times, which also results in the complete dye degradation closely approaching 15 min. After that, a large gap indicating a stronger decrease of catalytic efficiency occurs at 25th use, followed with a faster decay of catalytic efficiency than 4th to 23th use. Although the MG matrix composite can be reused for 45 times, the full decolorization of BR3B-A dye has been decreased from 10 min at the 1 st use to 30 min at the 45th use (reaction curves from 20 min to 30 min not shown in Fig. 3b). To distinguish these behaviors in the Fenton-like process, we employ curves from black to red to blue in color to represent three different stages of catalytic decay of MG matrix composite during recycling experiments, as shown in Fig. 3b.

On the other hand, the reusability of SLM-produced Fe-based MG matrix composite has also been performed in the sulfate radical-based reaction using PS under the same conditions. The reaction rate is even faster in the sulfate radical-based reaction with about 90 % dye removal rate at the 2 min of 1 st use than in the Fenton-like process. More importantly, although a significant decrease of reaction rate can be observed after the 1 st use, the degradation efficiency of BR3B-A almost remains constant at the following 44 reused times, with over 95 % removal rate at 5 min and almost complete removal at 10 min. This ultra-stable reusability of MG matrix composite in sulfate radical-based reaction gives the fact that it holds the highest reusability with promising efficiency among different catalysts as of now, and it can be further extended to higher reusability. In order to observe the change of degradation efficiency and catalytic ability of MG matrix composite, Fig. 3d and e show the dye removal rate of two systems at 5 and 10 min. Comparing to the progressive decrease of efficiency in Fenton-like process, the nearly unchangeable efficiency after being reused for 45 times has been clearly shown in the sulfate radical-based reaction. This behavior has also been demonstrated by $Fe_{78}Si_9B_{13}$ MG ribbons with being reused for 30 times [22] and very recently reported $Fe_{83}Si_2B_{11}P_3C_1$ MG ribbons with remarkable reusability at the 33 times before detrimental catalytic performance occurs, which is attributed to the uniquely in-situ self-reconstructed hierarchical gradient microstructure of MG ribbons during catalytic degradation [25].

3.2. Microstructure and surface evolution

In order to find out the intrinsic characteristics of SLM-produced Fe-based MG matrix composite in this work, the structural and surface evolution were investigated. Laser scan speed has already been considered as an important processing parameter during SLM process. It is known that laser energy density (E), which affects the densification and quality of SLM-produced component, can be defined as, $E = P/(v{\cdot}t{\cdot}s)$ [43], where P is the laser power (W), v is the laser scan speed (mm/s), t is the layer thickness (mm) and s is scan spacing (mm). Given that laser power, layer thickness and scan spacing were fixed in this work, a general lower scan speed will contribute to a higher laser energy density and vice versa [44]. Fig. 4a shows that all the SLM-produced components with different scan speeds present main amorphous features with slight crystalline peaks. Those crystalline peaks well match α-Fe phase at $2\theta = 52.5^\circ$, 77.6° and 100.1°, corresponding (011), (002) and (112) planes, respectively. In addition, Fe_2B phase can be identified from peak analysis, indicating that SLM process induces the generation of Fe_2B phase after solidification. Noting the composite nature of powder used in this work (Fig. 1b), the amorphous-crystalline nature of composite powder has been well maintained in the SLM-produced composites with different scan speeds. Fig. 4a inset suggests that the volume fraction (V_f) of amorphous phase (or crystalline phases) in the MG matrix composites varies with changing the laser scan speed and the composite manufactured at scan speed of 2000 mm/s shows the highest V_f with amorphous phase. The obtained results between V_f of amorphous phase and laser scan speed are reasonable because the amorphous phase in the powder would be more stable in the low energy input of laser and the solidification process by SLM may not be fast enough to vitrify melted powder into glass [45]. However, this seems to be closely related to the catalytic behavior in Fig. 3a. That is, a higher V_f of amorphous phase leads to an enhanced catalytic performance in the SLM-produced Fe-based MG matrix composite.

Fig. 4b shows the surface morphology of as-produced Fe-based MG matrix composite by SLM with laser scan speed of 2000 mm/s.

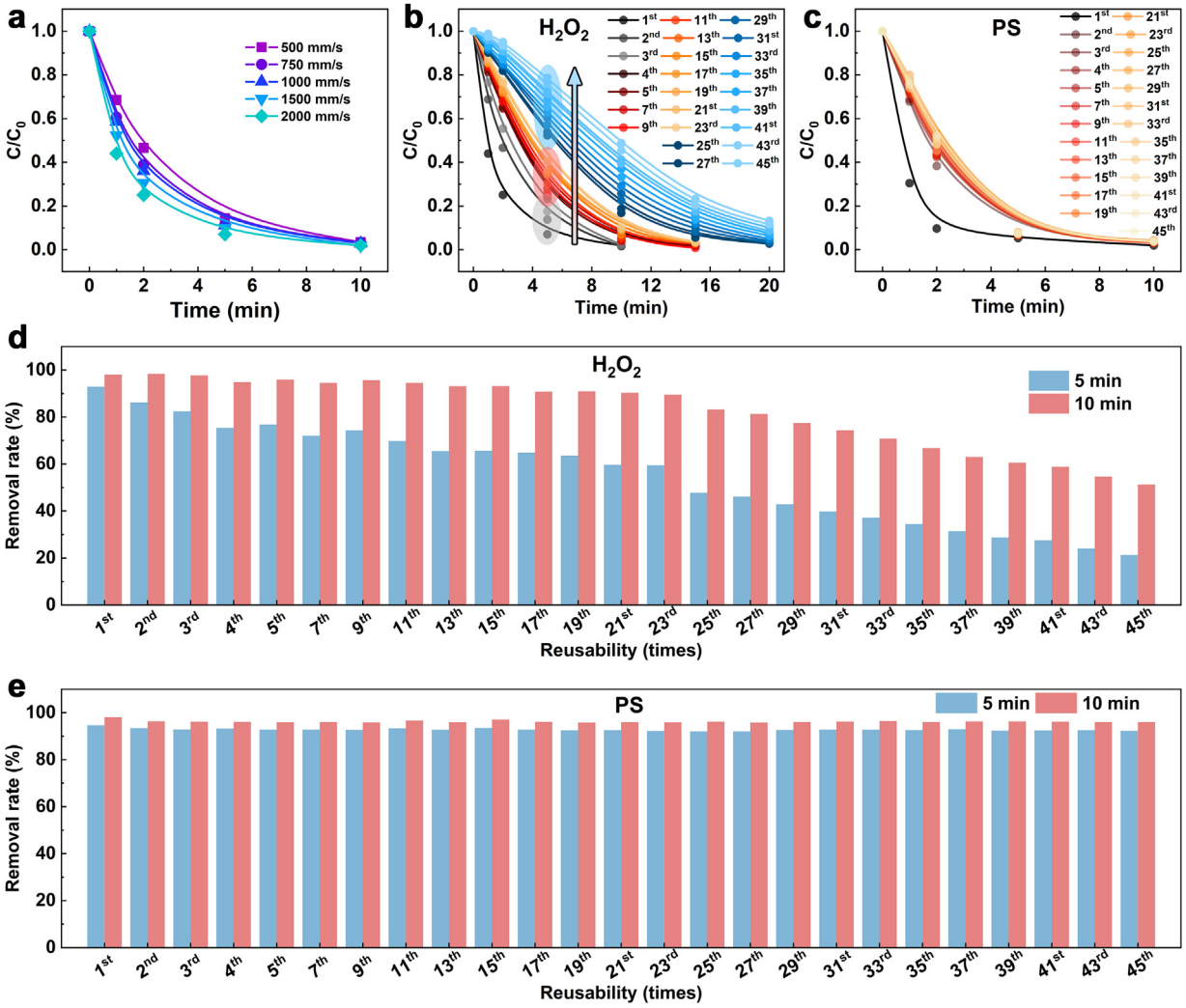

Fig. 3. (a) Effect of laser scan speed on the catalytic performance of SLM-produced Fe-based MG matrix composite in the Fenton-like process. (b) The reusability (up to 45 times) of SLM-produced Fe-based MG matrix composite (at laser scan speed of 2000 mm/s) in (b) Fenton-like process (H_2O_2) and (c) sulfate radical-based reaction (PS) for degrading BR3B-A dye (peroxide concentration: 1 mM, dye concentration: 20 ppm). (d) and (e) are corresponding dye removal rates of (b) and (c), respectively, at 5 and 10 min.

As aforementioned low energy input at a high laser scan speed, there are some unmelted powder exposed and attached to the surface. The porous microstructure (~500 μm pore diameter) can be clearly seen with a rough surface on the scaffold, providing a large contact area between porous composite and peroxides. Thus, it is reasonable to believe that the SLM-produced porous microstructure with a larger surface active site can induce ultra-fast degradation rates in the two different systems. After reused for 45 times in the Fenton-like system, Fig. 4c shows that the surface of SLM-produced porous MG matrix composite is fully covered with large amounts of reaction products, especially for the gaps on the scaffold. The zoom-in view (Fig. 4d) indicates that there is a thick after-reacted layer covered on the surface with many small bubble-like products, which are the aggregates during the reaction of recycling experiments. However, Fig. 4e shows that the surface reused for 45 times in the sulfate radical-based reaction is still fresh as as-produced MG matrix composite. This is further supported by the zoom-in view in Fig. 4f, where only a very thin layer covers on the surface. These distinct surface behaviors after reusing MG matrix composite for 45 times provide an astonishing result, since the after-reacted surface of catalyst during wastewater treatment is usually overlaid with products by adsorption, precipitation, etc. The oxide layer would grow by surface corrosion with a long processing time [46,47]. Especially, the degradation process for dyes usually accompanies with many intermediates and by-products [48].

However, the different surface morphologies between two systems provide solid evidences why the Fenton-like process has a detrimental effect on the reusability of MG matrix composite while the sulfate radical-based reaction remains its strong reusability even after reused for 45 times. Accordingly, the distinct surface behavior may largely dominate the catalytic behavior during recycling experiments. That is, the surface of MG matrix composite is easily involved and the intermediates/products during reactions tend to deposit on the catalyst surface to inhibit further catalytic activity in the Fenton-like process. The detrimental surface effect in the Fenton-like process has also been observed in other MG ribbons [23,36,42]. On the other hand, although SLM-produced porous MG matrix composite provides an iron source to activate PS in the sulfate radical-based reaction, the surface seems to release Fe ions without involvement of degradation reaction on the surface, or the surface product is cleaned during the reaction. Given that the catalyst and dye are the same in two systems, the only difference is the generation of hydroxyl radical ($^{\bullet}OH$) from Fenton-like process and sulfate radical ($SO_4^{\bullet -}$) from sulfate radical-based reaction [49,50].

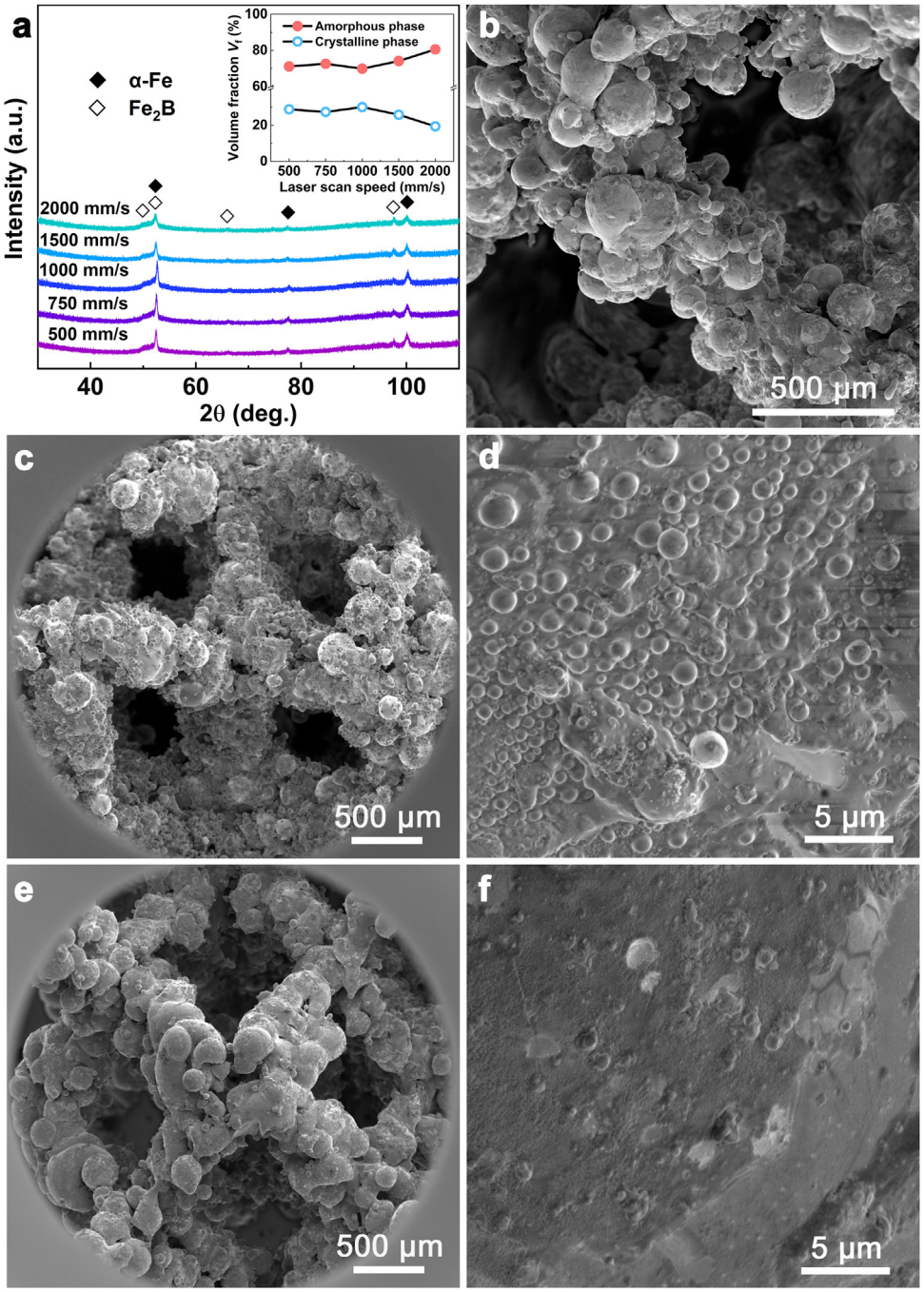

Fig. 4. (a) XRD patterns of SLM-produced Fe-based MG matrix composite based on laser scan speeds from 500 mm/s to 2000 mm/s. Inset shows the variation of volume fraction (V_f) of amorphous phase and crystalline phase according to the laser scan speed. (b) SEM micrograph of as-produced Fe-based MG matrix composite with porous microstructure. SEM micrographs of after-reacted porous Fe-based MG matrix composite in the (c), (d) Fenton-like process (H_2O_2) and in the (e), (f) sulfate radical-based reaction (PS).

Therefore, in this work, the possible reasons of SLM-produced porous Fe-based MG matrix composite to sustainably activate PS can summarize as follows: (1) SLM-produced porous MG matrix composite is corroded to release Fe ions, with activation of PS in the solution; (2) the degradation of dye occurs in the solution instead of on the surface of composite; (3) $SO_4^{\bullet -}$ may have the function to degrade generated products on the surface of composite to maintain fresh surface. However, the actual situation between the difference of two AOPs may be more complicated, where the intrinsic mechanism is still unknown to us at the current stage, but it would be interesting to be further investigated in the future. In this work, the significance mainly focuses on the catalytic performance of advanced materials with 3D printing and novel dual-phase structure at the cutting edge.

3.3. *Microstructural effect on catalytic performance*

Simultaneously, the microstructural change in the material containing amorphous phase is usually considered as an important characteristic during catalytic activity. Especially, the electron transfer efficiency of MG was reported to be highly inhibited when more crystalline phases were transformed from amorphous phase

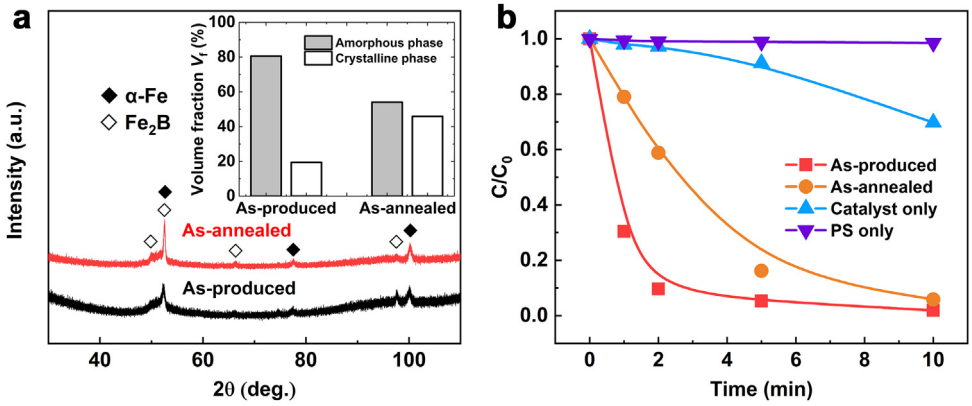

Fig. 5. (a) XRD patterns and (b) catalytic performance of as-produced and as-annealed (at 550°) porous Fe-based MG matrix composite by SLM at scan speed of 2000 mm/s. Inset of (a) shows the change of volume fraction (V_f) of amorphous and crystalline phase after annealing.

[19]. The declined catalytic performance, in fact, also occurs in the MG with microstructural relaxation due to the decrease of energy level and a tendency from metastable to equilibrium state [14]. In this work, the SLM-produced porous Fe-based MG matrix composite was subjected to the thermal treatment (550 °C) just at the temperature slightly higher than the onset crystallization based on DSC curve (540 °C, Fig. 1b inset). As can be seen from Fig. 5a, the annealing treatment contributes to a more intense crystallization peak of 2θ = 52.5°, indicating more α-Fe crystallines have been transformed from amorphous phase [31]. As a result, the residual amorphous phase becomes less in the annealed composite. The measured V_f of amorphous phase has decreased from 80 % to 54 % (Fig. 5a inset) after annealing. However, as suggested, the annealing temperature is still located at the region before recrystallization. There is no full crystallization observed in Fig. 5a and the SLM-produced porous MG matrix composite is still with amorphous-crystalline dual phase. This annealing-induced microstructural change of composite is further investigated for the effect of catalytic performance.

Fig. 5b shows that the as-produced composite has an extremely higher catalytic efficiency than its as-annealed counterpart. The as-produced composite achieves exceeding 90 % dye removal rate in 2 min, while only 40 % removal rate is observed for the as-annealed counterpart with the same period of time. It is worth to note that the use of sole PS or catalyst (SLM-produced MG matrix composite) results in limited dye removal efficiency, indicating the ultra-strong catalytic ability of MG matrix composite in the sulfate radical-based reaction. Obviously, more amorphous phase in the MG matrix composite easily induces a higher catalytic behavior than the annealed counterpart with more crystalline phase in this work, suggesting the V_f of crystalline phase in the composite microstructure should be controlled at a low level to achieve high efficiency of interfacial electron transfer. The function of α-Fe nanocrystals could serve as a trigger of easy electron transfer but a large amount of α-Fe lead to an inhibitive effect. It is known that the crystallization and/or microstructural relaxation would also have a detrimental effect on the electron transfer (charge transfer) efficiency of amorphous alloys [14]. In this work, the energy level change is also considered as one of the reasons for the decay of dye degradation in the sulfate radical-based reaction.

3.4. Assessment of overall catalytic ability

Although the reaction rate constant k_{obs} can partly reflect an activation efficiency of catalyst during AOPs, this is highly affected by various parameters (catalyst dosage, temperature, peroxide concentration, etc.). As such, the activation energy ΔE is usually considered as an indicator for catalyst to pass energy barrier of reaction. That is, a lower ΔE contributes to an easier occurrence of catalytic behavior. The ΔE is obtained by the Arrhenius equation: $ln\,k_{obs} = -\Delta E/RT + lnA$, where R is the gas constant (8.314 J/(mol·K)) and A is a pre-exponential factor. However, most of the time, a lower ΔE in a catalyst does not represent that the catalytic reaction can be completed faster than the one with a higher ΔE in the same conditions. This is because the reaction may be also affected by their internal and surface microstructure. The catalytic efficiency under optimized conditions may vary. Therefore, in order to assess the overall catalytic ability of SLM-produced porous Fe-based MG matrix composite, this work considers the ΔE together with k_{obs} under optimized conditions and it is compared with different catalysts in Fig. 6 and Table 1. The k_{obs} is selected under optimized conditions due to variation of experimental conditions based on different catalysts (reports). According to Table 1, the k_{obs} is referenced or calculated with conditions at room temperature unless specified. Here, solid and hollow symbols are used to distinguish the reaction using AOPs or not due to catalytic advantages of transition-metal-based catalysts in AOPs. These materials are usually used in the AOPs to accelerate the catalytic degradation of organic pollutants.

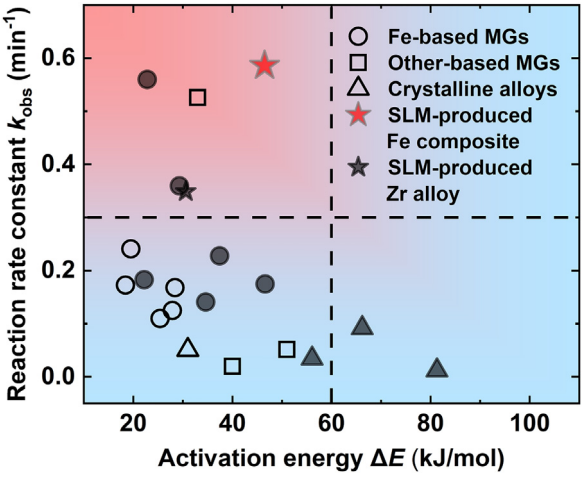

Fig. 6. Overall catalytic ability for different catalysts. The solid and hollow symbols represent if the catalyst was used in the AOPs or not, respectively. The data were obtained from Table 1.

Fig. 6 summarizes the values for k_{obs} and ΔE in Fe/Mg/Co/Al-based MGs, crystalline alloys and SLM-produced alloys. Given that crystalline metal-based catalysts usually have ΔE between 60–250 kJ/mol [25], the k_{obs} does not present a high catalytic effi-

Table 1
Comparison of intrinsic kinetic characteristic (activation energy ΔE) versus external catalytic performance (reaction rate constant k_{obs}) for different catalysts.

Catalyst		Pollutants	Activation energy, ΔE (kJ/mol)	AOPs or not	Reaction rate constant, k_{obs} (min^{-1})	Ref.
Fe-based MGs	$Fe_{84}B_{16}$	Direct blue 6	25.4	No	0.110	[53]
	$Fe_{80}B_{20}$	Direct blue 15	37.4	Yes	0.228	[54]
	$Fe_{78}(Si, B)_{22}$	Orange II	27.9	No	0.125	[55]
	$Fe_{80}P_{13}C_7$	Methylene blue	22.8	Yes	0.56	[23]
	$Fe_{68}Co_{10}Si_8B_{14}$	Acid orange II	18.4	No	0.173	[56]
	$(Fe_{0.99}Mo_{0.01})_{78}Si_9B_{13}$	Acid orange II	28.4	No	0.168	[57]
	$Fe_{76}Si_9B_{10}P_5$	Direct blue	19.5	No	0.241	[58]
	$Fe_{72}Si_2B_{20}Nb_6$	Direct blue 15	34.6	Yes	0.141	[59]
	$Fe_{50}Ni_{30}P_{13}C_7$	Brilliant black BN	46.6	Yes	0.175	[32]
	$Fe_{83}Si_2B_{11}P_3C_1$	Rhodamine B	29.3	Yes	0.360	[25]
	$Fe_{73.5}Si_{13.5}B_9Cu_1Nb_3$	Eosin Y	22.2	Yes	0.183	[60]
Other-based MGs	$Al_{85}Ni_9Y_6$	Direct blue 2B	40	No	0.020 (30°)	[61]
	$Co_{78}Si_8B_{14}$	Acid orange II	33	No	0.526	[52]
	$Mg_{73}Zn_{21.5}Ca_{5.5}$	Five dyes	51	No	0.052	[51]
	Co_3O_4	Phenol	66.2	Yes	0.092	[62]
Crystalline alloys	Fe_2O_3-ZSM-5	M-cresol	81.3	Yes	0.0125 (40°)	[63]
	Fe-Carbon aerogel	Orange II	56.1	Yes	0.0346 (30°)	[64]
	Hydroxyl-Fe pillared bentonite	Acid light yellow G	31.0	No	0.051 (30°)	[65]
SLM-produced alloys	$Fe_{70}Cr_5Ni_3Mo_3W_9Si_5B_5$	Cibacron brilliant red 3B-A	46.5	Yes	0.586	This work
	$Zr_{55}Cu_{30}Ni_5Al_{10}$	Methyl orange	30.6	Yes	0.349 (45°)	[41]

ciency although some of them are used in the AOPs. On the other hand, MGs always locate at the region with low ΔE (<60 kJ/mol) and most of them have 1.5–2.0 times higher reaction rate than crystalline metal-based catalysts. The MGs have been considered as superior alternatives of crystalline catalysts [19,51,52]. However, SLM-produced catalysts hold the promise with a low ΔE and a high k_{obs} which makes the composite locate at the red region (catalysts with high overall catalytic ability) in the Fig. 6. Especially, the SLM-produced Fe-based MG matrix composite in this work has an extremely high k_{obs} (0.586 min^{-1}) than the SLM-produced Zr alloy (0.349 min^{-1}). The slightly high ΔE (46.5 kJ/mol) may be attributed to the dual-phase nature of SLM-produced Fe-based MG matrix composite, but it is still lower than most of crystalline catalysts, indicating the strong overall catalytic ability in SLM-produced Fe-based MG matrix composite. In this case, the SLM-produced Fe-based MG matrix composite is also expected to exploit its superiority in the purification of inorganic pollutants, which has been demonstrated by Fe-based MG ribbons recently [66], and this would further promote its practical application ability in future.

4. Conclusions

In this work, porous Fe-based metallic glass (MG) matrix composites with a rhombic dodecahedron microstructure are manufactured by selective laser melting (SLM), which is then applied in the catalytic degradation of cibacron brilliant red 3B-A (BR3B-A) dye solution. The SLM-produced Fe-based MG matrix composite has a dual-phase microstructure composed of amorphous phase and crystalline phase. The comparative degradation of MG matrix composite in Fenton-like and in sulfate radical-based reactions suggests the highest reusability of catalyst with remarkable efficiency as of now. The reusability of in MG matrix composite in sulfate radical-based reaction (using sodium persulfate (PS)) is demonstrated with up to 45 times without losing any apparent catalytic efficiency. The detrimental surface decay is responsible for the decreased efficiency when reusing MG matrix composite in Fenton-like -process, while the surface morphology of MG matrix composite remains fresh in sulfate radical-based reaction although it is reused for 45 times, indicating there is a distinct catalytic mechanism in these two AOPs and sulfate radical-based reaction is more desirable in the practical application. More importantly, the SLM-produced porous Fe-based MG matrix composite has a superior overall catalytic ability with high reaction rate constant and low activation energy than other catalysts. The reported reusability and overall catalytic ability in SLM-produced porous Fe-based MG matrix composite hold the promise to design new generation catalyst approaching practical application and high economic value.

Acknowledgment

Financial supports from Australian Research Council through Discovery Project (DP130103592) and National Science Foundation of China (Grant No. 51771103) are gratefully acknowledged.

References

[1] L.C. Zhang, Y.J. Liu, S. Li, Y. Hao, Additive manufacturing of titanium alloys by electron beam melting: a review, Adv. Eng. Mater. 20 (2018), 1700842.
[2] Y.J. Liu, S.J. Li, L.C. Zhang, Y.L. Hao, T.B. Sercombe, Early plastic deformation behaviour and energy absorption in porous β-type biomedical titanium produced by selective laser melting, Scr. Mater. 153 (2018) 99–103.
[3] X. Zhou, C.J. Liu, Three-dimensional printing for catalytic applications: current status and perspectives, Adv. Funct. Mater. 27 (2017), 1701134.
[4] Y.J. Liu, H.L. Wang, S.J. Li, S.G. Wang, W.J. Wang, W.T. Hou, Y.L. Hao, R. Yang, L.C. Zhang, Compressive and fatigue behavior of beta-type titanium porous structures fabricated by electron beam melting, Acta Mater. 126 (2017) 58–66.
[5] X. Wei, D. Li, W. Jiang, Z. Gu, X. Wang, Z. Zhang, Z. Sun, 3D printable graphene composite, Sci. Rep. 5 (2015) 11181.
[6] C.R. Tubío, J. Azuaje, L. Escalante, A. Coelho, F. Guitián, E. Sotelo, A. Gil, 3D printing of a heterogeneous copper-based catalyst, J. Catal. 334 (2016) 110–115.
[7] J.E. Katz, T.R. Gingrich, E.A. Santori, N.S. Lewis, Combinatorial synthesis and high-throughput photopotential and photocurrent screening of mixed-metal oxides for photoelectrochemical water splitting, Energy Environ. Sci. 2 (2009) 103–112.
[8] H. Thakkar, S. Eastman, A. Hajari, A.A. Rownaghi, J.C. Knox, F. Rezaei, 3D-printed zeolite monoliths for CO_2 removal from enclosed environments, ACS Appl. Mater. Interfaces 8 (2016) 27753–27761.
[9] E. Fantino, A. Chiappone, I. Roppolo, D. Manfredi, R. Bongiovanni, C.F. Pirri, F. Calignano, 3D printing of conductive complex structures with in situ generation of silver nanoparticles, Adv. Mater. 28 (2016) 3712–3717.
[10] P. Michorczyk, E. Hędrzak, A. Węgrzyniak, Preparation of monolithic catalysts using 3D printed templates for oxidative coupling of methane, J. Mater. Chem. A Mater. Energy Sustain. 4 (2016) 18753–18756.

[11] C.Y. Lee, A.C. Taylor, S. Beirne, G.G. Wallace, 3D-printed conical arrays of TiO_2 electrodes for enhanced photoelectrochemical water splitting, Adv. Energy Mater. 7 (2017), 1701060.
[12] A. Ambrosi, J.G.S. Moo, M. Pumera, Helical 3D-printed metal electrodes as custom-shaped 3D platform for electrochemical devices, Adv. Funct. Mater. 26 (2016) 698–703.
[13] A. Avril, C.H. Hornung, A. Urban, D. Fraser, M. Horne, J.P. Veder, J. Tsanaktsidis, T. Rodopoulos, C. Henry, D.R. Gunasegaram, Continuous flow hydrogenations using novel catalytic static mixers inside a tubular reactor, React. Chem. Eng. 2 (2017) 180–188.
[14] S.X. Liang, Z. Jia, Y.J. Liu, W. Zhang, W. Wang, J. Lu, L.C. Zhang, Compelling rejuvenated catalytic performance in metallic glasses, Adv. Mater. 30 (2018), 1802764.
[15] J.C. Qiao, Y. Yao, J.M. Pelletier, L.M. Keer, Understanding of micro-alloying on plasticity in Cu46Zr47−xAl7Dyx ($0 \leq x \leq 8$) bulk metallic glasses under compression: based on mechanical relaxations and theoretical analysis, Int. J. Plast. 82 (2016) 62–75.
[16] J.C. Qiao, Q. Wang, J.M. Pelletier, H. Kato, R. Casalini, D. Crespo, E. Pineda, Y. Yao, Y. Yang, Structural heterogeneities and mechanical behavior of amorphous alloys, Prog. Mater. Sci. 104 (2019) 250–329.
[17] L.C. Zhang, Z. Jia, F. Lyu, S.X. Liang, J. Lu, A review of catalytic performance of metallic glasses in wastewater treatment: recent progress and prospects, Prog. Mater. Sci. 105 (2019), 100576.
[18] J.Q. Wang, Y.H. Liu, M.W. Chen, G.Q. Xie, D.V. Louzguine-Luzgin, A. Inoue, J.H. Perepezko, Rapid degradation of azo dye by Fe-based metallic glass powder, Adv. Funct. Mater. 22 (2012) 2567–2570.
[19] Z. Jia, X. Duan, P. Qin, W. Zhang, W. Wang, C. Yang, H. Sun, S. Wang, L.C. Zhang, Disordered atomic packing structure of metallic glass: toward ultrafast hydroxyl radicals production rate and strong electron transfer ability in catalytic performance, Adv. Funct. Mater. 27 (2017), 1702258.
[20] F. Hu, S. Zhu, S. Chen, Y. Li, L. Ma, T. Wu, Y. Zhang, C. Wang, C. Liu, X. Yang, L. Song, X. Yang, Y. Xiong, Amorphous metallic NiFeP: a conductive bulk material achieving high activity for oxygen evolution reaction in both alkaline and acidic media, Adv. Mater. 29 (2017), 1606570.
[21] Y.C. Hu, Y.Z. Wang, R. Su, C.R. Cao, F. Li, C.W. Sun, Y. Yang, P.F. Guan, D.W. Ding, Z.L. Wang, W.H. Wang, A highly efficient and self-stabilizing metallic-glass catalyst for electrochemical hydrogen generation, Adv. Mater. 28 (2016) 10293–10297.
[22] Z. Jia, X. Duan, W. Zhang, W. Wang, H. Sun, S. Wang, L.C. Zhang, Ultra-sustainable $Fe_{78}Si_9B_{13}$ metallic glass as a catalyst for activation of persulfate on methylene blue degradation under UV-vis light, Sci. Rep. 6 (2016) 38520.
[23] Q. Wang, M. Chen, P. Lin, Z. Cui, C. Chu, B. Shen, Investigation of FePC amorphous alloys with self-renewing behaviour for highly efficient decolorization of methylene blue, J. Mater. Chem. A Mater. Energy Sustain. 6 (2018) 10686–10699.
[24] Q. Wang, L. Yun, M. Chen, D. Xu, Z. Cui, Q. Zeng, P. Lin, C. Chu, B. Shen, Competitive effects of structural heterogeneity and surface chemical states on catalytic efficiency of FeSiBPCu amorphous and nanocrystalline alloys, ACS Appl. Nano Mater. 2 (2019) 214–227.
[25] Z. Jia, Q. Wang, L. Sun, Q. Wang, L.C. Zhang, G. Wu, J.H. Luan, Z.B. Jiao, A. Wang, S.X. Liang, M. Gu, J. Lu, Attractive in situ self-reconstructed hierarchical gradient structure of metallic glass for high efficiency and remarkable stability in catalytic performance, Adv. Funct. Mater. 29 (2019), 1807857.
[26] C. Lv, C. Yan, G. Chen, Y. Ding, J. Sun, Y. Zhou, G. Yu, An amorphous noble-metal-free electrocatalyst that enables nitrogen fixation under ambient conditions, Angew. Chem. Int. Ed. 57 (2018) 6073–6076.
[27] Y. Jin, R. Li, H. Xu, X.B. Chen, T. Zhang, A new strategy to fabricate nanoporous iron-based metallic glasses: selective phase tailoring of amorphous-nanocrystalline composite alloys through electrochemical dissolution, Scr. Mater. 133 (2017) 14–18.
[28] C. Yang, C. Zhang, W. Xing, L. Liu, 3D printing of Zr-based bulk metallic glasses with complex geometries and enhanced catalytic properties, Intermetallics 94 (2018) 22–28.
[29] Z. Jia, S.X. Liang, W.C. Zhang, W.M. Wang, C. Yang, L.C. Zhang, Heterogeneous photo Fenton-like degradation of cibacron brilliant red 3b-A dye using amorphous $Fe_{78}Si_9B_{13}$ and $Fe_{73.5}Si_{13.5}B_9Cu_1Nb_3$ alloys: the influence of adsorption, J. Taiwan Inst. Chem. Eng. 71 (2017) 128–136.
[30] L.C. Zhang, S.X. Liang, Fe-based metallic glasses in functional catalytic applications, Chem. Asian J. 13 (2018) 3575–3592.
[31] Z. Jia, J.C. Wang, S.X. Liang, W.C. Zhang, W.M. Wang, L.C. Zhang, Activation of peroxymonosulfate by $Fe_{78}Si_9B_{13}$ metallic glass: the influence of crystallization, J. Alloys Compd. 728 (2017) 525–533.
[32] S.X. Liang, W. Zhang, W. Wang, G. Jia, W. Yang, L.C. Zhang, Surface reactivation of FeNiPC metallic glass: a strategy for highly enhanced catalytic behavior, J. Phys. Chem. Solids 132 (2019) 89–98.
[33] J.C. Wang, Y.J. Liu, P. Qin, S.X. Liang, T.B. Sercombe, L.C. Zhang, Selective laser melting of Ti–35Nb composite from elemental powder mixture: microstructure, mechanical behavior and corrosion behavior, Mater. Sci. Eng. A 760 (2019) 214–224.
[34] Y.J. Liu, Z. Liu, Y. Jiang, G.W. Wang, Y. Yang, L.C. Zhang, Gradient in microstructure and mechanical property of selective laser melted AlSi10Mg, J. Alloys Compd. 735 (2018) 1414–1421.
[35] Y.J. Liu, Y.S. Zhang, L.C. Zhang, Transformation-induced plasticity and high strength in beta titanium alloy manufactured by selective laser melting, Materialia 6 (2019), 100299.
[36] L. Hou, Q. Wang, X. Fan, F. Miao, W. Yang, B. Shen, Effect of Co addition on catalytic activity of FePCCu amorphous alloy for methylene blue degradation, New J. Chem. 43 (2019) 6126–6135.
[37] X.F. Li, S.X. Liang, X.W. Xi, Z. Jia, S.K. Xie, H.C. Lin, J.P. Hu, L.C. Zhang, Excellent performance of $Fe_{78}Si_9B_{13}$ metallic glass for activating peroxymonosulfate in degradation of naphthol green B, Metals 7 (2017) 273.
[38] S.X. Liang, Z. Jia, W.C. Zhang, W.M. Wang, L.C. Zhang, Rapid malachite green degradation using $Fe_{73.5}Si_{13.5}B_9Cu_1Nb_3$ metallic glass for activation of persulfate under UV–vis light, Mater. Des. 119 (2017) 244–253.
[39] W. Yang, Q. Wang, W. Li, L. Xue, H. Liu, J. Zhou, J. Mo, B. Shen, A novel thermal-tuning Fe-based amorphous alloy for automatically recycled methylene blue degradation, Mater. Des. 161 (2019) 136–146.
[40] Z. Jia, F. Lyu, L.C. Zhang, S. Zeng, S.X. Liang, Y.Y. Li, J. Lu, Pt nanoparticles decorated heterostructured g-C_3N_4/Bi_2MoO_6 microplates with highly enhanced photocatalytic activities under visible light, Sci. Rep. 9 (2019) 7636.
[41] C. Yang, C. Zhang, L. Liu, Excellent degradation performance of 3D hierarchical nanoporous structures of copper towards organic pollutants, J. Mater. Chem. A Mater. Energy Sustain. 6 (2018) 20992–21002.
[42] Z. Jia, J. Kang, W.C. Zhang, W.M. Wang, C. Yang, H. Sun, D. Habibi, L.C. Zhang, Surface aging behaviour of Fe-based amorphous alloys as catalysts during heterogeneous photo Fenton-like process for water treatment, Appl. Catal. B 204 (2017) 537–547.
[43] L. Thijs, F. Verhaeghe, T. Craeghs, J.V. Humbeeck, J.P. Kruth, A study of the microstructural evolution during selective laser melting of Ti–6Al–4V, Acta Mater. 58 (2010) 3303–3312.
[44] Y.J. Liu, S. Li, W. Hou, S. Wang, Y. Hao, R. Yang, T.B. Sercombe, L.C. Zhang, Electron beam melted beta-type Ti–24Nb–4Zr–8Sn porous structures with high strength-to-modulus ratio, J. Mater. Sci. Technol. 32 (2016) 505–508.
[45] S. Pauly, L. Löber, R. Petters, M. Stoica, S. Scudino, U. Kühn, J. Eckert, Processing metallic glasses by selective laser melting, Mater. Today 16 (2013) 37–41.
[46] L.Y. Chen, P. Shen, L. Zhang, S. Lu, L. Chai, Z. Yang, L.C. Zhang, Corrosion behavior of non-equilibrium Zr-Sn-Nb-Fe-Cu-O alloys in high-temperature 0.01 M LiOH aqueous solution and degradation of the surface oxide films, Corros. Sci. 136 (2018) 221–230.
[47] L.Y. Chen, J. Li, Y. Zhang, W. Lu, L.C. Zhang, L. Wang, D. Zhang, Effect of low-temperature pre-deformation on precipitation behavior and microstructure of a Zr-Sn-Nb-Fe-Cu-O alloy during fabrication, J. Nucl. Sci. Technol. 53 (2016) 496–507.
[48] Z. Jia, L.B.T. La, W.C. Zhang, S.X. Liang, B. Jiang, S.K. Xie, D. Habibi, L.C. Zhang, Strong enhancement on dye photocatalytic degradation by ball-milled TiO_2: a study of cationic and anionic dyes, J. Mater. Sci. Technol. 33 (2017) 856–863.
[49] J.C. Wang, S.X. Liang, Z. Jia, W.C. Zhang, W.M. Wang, Y.J. Liu, J. Lu, L.C. Zhang, Chemically dealloyed Fe-based metallic glass with void channels-like architecture for highly enhanced peroxymonosulfate activation in catalysis, J. Alloys Compd. 785 (2019) 642–650.
[50] S.X. Liang, Z. Jia, W.C. Zhang, X.F. Li, W.M. Wang, H.C. Lin, L.C. Zhang, Ultrafast activation efficiency of three peroxides by $Fe_{78}Si_9B_{13}$ metallic glass under photo-enhanced catalytic oxidation: a comparative study, Appl. Catal. B 221 (2018) 108–118.
[51] J.Q. Wang, Y.H. Liu, M.W. Chen, D.V. Louzguine-Luzgin, A. Inoue, J.H. Perepezko, Excellent capability in degrading azo dyes by MgZn-Based metallic glass powders, Sci. Rep. 2 (2012) 418.
[52] X.D. Qin, Z.W. Zhu, G. Liu, H.M. Fu, H.W. Zhang, A.M. Wang, H. Li, H.F. Zhang, Ultrafast degradation of azo dyes catalyzed by cobalt-based metallic glass, Sci. Rep. 5 (2015) 18226.
[53] Y. Tang, Y. Shao, N. Chen, K.F. Yao, Rapid decomposition of direct blue 6 in neutral solution by Fe-B amorphous alloys, RSC Adv. 5 (2015) 6215–6221.
[54] R. Li, X.J. Liu, H. Wang, Y. Wu, K.C. Chan, Z.P. Lu, Flexible glassy grid structure for rapid degradation of azo dye, Mater. Des. 155 (2018) 346–351.
[55] C. Zhang, Z. Zhu, H. Zhang, Z. Hu, Rapid reductive degradation of azo dyes by a unique structure of amorphous alloys, Chin. Sci. Bull. 56 (2011) 3988–3992.
[56] C. Zhang, Z. Zhu, H. Zhang, Effects of the addition of Co, Ni or Cr on the decolorization properties of Fe-Si-B amorphous alloys, J. Phys. Chem. Solids 110 (2017) 152–160.
[57] C. Zhang, Z. Zhu, H. Zhang, Z. Hu, On the decolorization property of Fe–Mo–Si–B alloys with different structures, J. Non-Cryst. Solids 358 (2012) 61–64.
[58] N. Weng, F. Wang, F. Qin, W. Tang, Z. Dan, Enhanced azo-dyes degradation performance of Fe-Si-B-P nanoporous architecture, Materials 10 (2017) 1001.
[59] Z. Deng, X.H. Zhang, K.C. Chan, L. Liu, T. Li, Fe-based metallic glass catalyst with nanoporous surface for azo dye degradation, Chemosphere 174 (2017) 76–81.
[60] J.C. Wang, Z. Jia, S.X. Liang, P. Qin, W.C. Zhang, W.M. Wang, T.B. Sercombe, L.C. Zhang, $Fe_{73.5}Si_{13.5}B_9Cu_1Nb_3$ metallic glass: rapid activation of peroxymonosulfate towards ultrafast eosin Y degradation, Mater. Des. 140 (2018) 73–84.
[61] P. Wang, J.Q. Wang, H. Li, H. Yang, J. Huo, J. Wang, C. Chang, X. Wang, R.W. Li, G. Wang, Fast decolorization of azo dyes in both alkaline and acidic solutions by Al-based metallic glasses, J. Alloys Compd. 701 (2017) 759–767.
[62] E. Saputra, S. Muhammad, H. Sun, H.M. Ang, M.O. Tadé, S. Wang, A comparative study of spinel structured Mn_3O_4, Co_3O_4 and Fe_3O_4

nanoparticles in catalytic oxidation of phenolic contaminants in aqueous solutions, J. Colloid Interface Sci. 407 (2013) 467–473.
[63] Y. Yang, H. Zhang, Y. Yan, The preparation of Fe_2O_3-ZSM-5 catalysts by metal-organic chemical vapour deposition method for catalytic wet peroxide oxidation of m-cresol, R. Soc. Open Sci. 5 (2018), 171731.
[64] J.H. Ramirez, F.J. Maldonado-Hódar, A.F. Pérez-Cadenas, C. Moreno-Castilla, C.A. Costa, L.M. Madeira, Azo-dye orange II degradation by heterogeneous Fenton-like reaction using carbon-Fe catalysts, Appl. Catal. B 75 (2007) 312–323.
[65] J. Chen, L. Zhu, Heterogeneous UV-Fenton catalytic degradation of dyestuff in water with hydroxyl-Fe pillared bentonite, Catal. Today 126 (2007) 463–470.
[66] S.X. Liang, W. Zhang, L. Zhang, W. Wang, L.C. Zhang, Remediation of industrial contaminated water with arsenic and nitrate by mass-produced Fe-based metallic glass: toward potential industrial applications, Sustain. Mater. Technol. 22 (2019), e00126.